JOURNAL OF CATALYSIS 50, 279–290 (1977)

Interaction of Hydrogen, Carbon Monoxide, and Formaldehyde with Ruthenium

D. WAYNE GOODMAN,[1] THEODORE E. MADEY, MASATOSHI ONO,[2] AND JOHN T. YATES, JR.

Surface Processes and Catalysis Section, National Bureau of Standards, Washington, D.C. 20234

Received March 10, 1977; revised July 7, 1977

The interaction of H_2, CO, and H_2CO with a clean (110) ruthenium surface has been studied using temperature-programmed desorption methods. Although Ru is known to be an excellent catalyst for methane production via hydrogenation of CO, no observable CH_4 was produced over Ru(110) at $H_2 + CO$ pressures up to $\sim 10^{-3}$ Torr, due to kinetic limitations. Also, no CH_4 was observed to desorb from coadsorbed $H_2 + CO$. Formaldehyde dissociates upon adsorption on Ru(110) and yields H_2 and CO as the dominant desorption products. In addition, a small ($\sim 0.1\%$ of a monolayer) amount of CH_4 was also seen following H_2CO adsorption. This CH_4 presumably originates from the thermal decomposition of a low-concentration oxygenated hydrocarbon complex. The relationship between this complex and the catalytic intermediate in the methanation reaction is explored.

INTRODUCTION

Ruthenium catalysts are well known for their ability to catalyze the hydrogenation of carbon monoxide to produce methane (*1*). Many authors have concluded that surface intermediates such as the enol form of formaldehyde

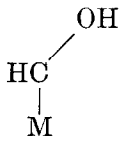

must be involved in the methanation reaction on transition metal catalysts such as Ru and Ni, but little or no direct information about surface intermediates of this type have been obtained (*2, 3*). It is surprising that experiments involving the adsorption and decomposition of formaldehyde on methanation catalysts have not been widely carried out to test mechanisms involving formaldehyde-derived intermediates.

Few studies of the chemistry of H_2CO adsorbed on metal surfaces have been reported to date. Several studies of formaldehyde chemistry on tungsten single-crystal surfaces have been conducted recently using thermal desorption, work function, and X-ray photoelectron spectroscopy techniques (*4–6*). Basically it has been found that small yields of CH_4 and CO_2 may be obtained from adsorbed layers on tungsten produced by formaldehyde adsorption, but that mixed layers of hydrogen and carbon monoxide do not yield detectable quantities of CH_4. It has not been possible to detect the intermediates responsible for CH_4 production using X-ray photoelectron spectroscopy, although a surface species related to CO_2 production was observed (*5*).

[1] NRC–NBS Postdoctoral Research Associate, 1976–1978.

[2] NBS Guest Worker. Permanent address: Electrotechnical Laboratory, Tanashi, Tokyo, Japan.

ISSN 0021-9517

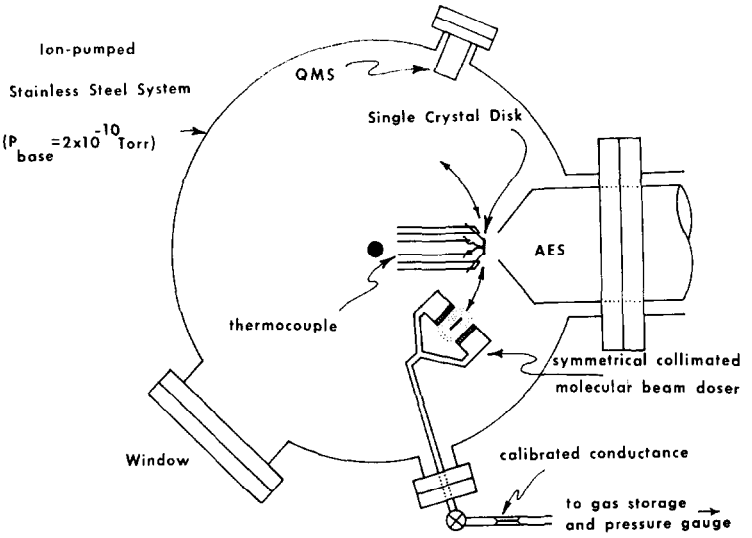

FIG. 1. Schematic of ultrahigh vacuum apparatus for Auger spectroscopy and thermal desorption studies from single-crystal catalysts. A QMS (quadrupole mass spectrometer) was used for partial pressure determinations. Total pressure was measured with a Bayard–Alpert gauge. The Ru crystal, mounted on a rotary manipulator, was heated resistively by the passage of ac current through Ru or W leads. AES, Auger electron spectrometer.

The present paper is concerned with the chemisorption of hydrogen and carbon monoxide by a single-crystal plane of Ru containing a high density of kinked Ru-atom rows at its surface, the Ru(110) surface.[3] A comparison of the chemistry of formaldehyde on this surface with that of hydrogen and carbon monoxide has been carried out in order to test whether formaldehyde-derived surface species exhibit unique chemical behavior. Of particular concern was whether or not the decomposition of H_2CO on Ru(110) yielded significantly more CH_4 as a desorption product than could be produced by coadsorption of H_2 and CO.

EXPERIMENTAL

These studies were carried out in a stainless steel ultrahigh vacuum chamber as shown in Fig. 1. A single-crystal wafer of Ru, (0.6-cm average diameter, 0.02-cm thick), polished to expose Ru(110) faces on both sides, could be electrically heated by the passage of ac current through either W or Ru mounting leads 0.05 cm in diameter. Changing from W to Ru support leads in separate experiments did not alter desorption product yields, etc. The temperature of the crystal could be monitored with a 97% W/3% Re–74% W/26% Re thermocouple (0.0125-cm-diameter wire). Comparison of the thermocouple emf with optical pyrometer readings indicated an average difference of ±8°K for 1300 K $< T <$ 1755 K.

A symmetrical collimated molecular beam doser, designed to deposit adsorbate uniformly on both faces of the single-crystal Ru, was used in these studies. The orifices were constructed of microchannel plate capillary arrays consisting of multiple parallel capillaries 0.0025 cm in diameter by 0.063 cm in length. This technique of adsorbing gas on the crystal effectively prevents a major gas load from being introduced into the ultrahigh vacuum

[3] We employ the three-digit notation to index single-crystal faces of h.c.p. Ru, rather than the redundant four-digit notation.

chamber, leading to unacceptable levels of residual gases. The flow of gases to this effusion source was controlled by adjusting the pressure behind a glass capillary conductor within the gas storage lines. It was found that the flux within the doser region was 40 times the random flux in the chamber (by using the rate of adsorption of CO on the crystal as a detector).

Following adsorption on the crystal, it was rotated to the region of the quadrupole mass spectrometer; the pumping speed to the ion pumps was reduced using a throttle valve, and the crystal was heated electrically while monitoring the partial pressure of a desorption product.

The Ru(110) crystal was cleaned by heating at $\sim$1500 K repeatedly in O_2 at $\sim 1 \times 10^{-5}$ Torr of O_2 beam pressure and than flashing clean *in vacuo* at 1515 K. Following this cleaning procedure, the Auger spectrum shown in Fig. 2 was obtained. The spectral features seen for clean Ru(110) were identical to the Auger spectra reported by Palmberg *et al.* (*7*). In addition, we observed a small and variable peak at 118 eV which may possibly be attributed to phosphorous impurity. Treatment in O_2 at $T \sim 1400$ K was found to reduce this 118-eV peak to small intensity. A similar cleaning procedure has been used previously for the Ru(001) surface (*8*).

The base pressure in the chamber was 2×10^{-10} Torr, with the major residual gases being H_2, CH_4, and CO. The quadrupole mass spectrometer was operated at an electron energy of 70 eV in all measurements.

RESULTS

A series of flash-desorption spectra for CO on Ru(110) (*9*) are shown in Fig. 3. The curves, each corresponding to a different CO exposure, are displaced vertically for clarity. The CO pressure change, as observed by the QMS ion current at mass 28, is plotted as a function of temperature. The area under each curve is proportional to the CO coverage. These spectra indicate that the CO binding energy decreases with increasing θ_{CO}. This decrease may be due to repulsive interactions in the adlayer at higher coverages or to the population of a second unresolved binding mode. Assuming first-order kinetics for CO desorption and a normal pre-exponential factor, 1×10^{12} sec^{-1}, the approximate range of activation energies for CO desorption, based on desorption peak temperatures, varies from

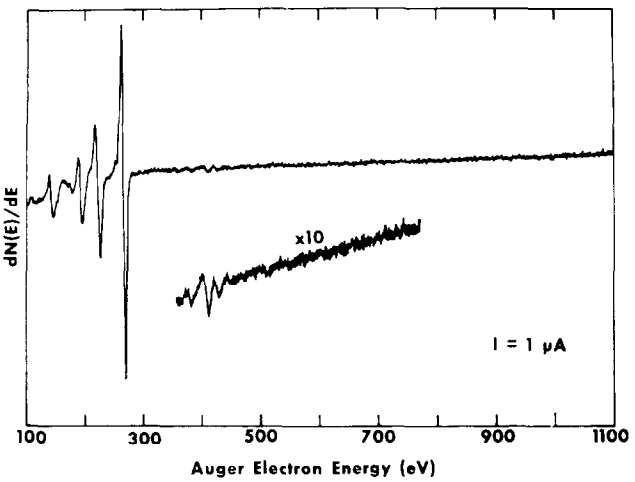

FIG. 2. Auger electron spectrum of clean Ru(110) following O_2 cleaning and heating *in vacuo* to 1515 K. Modulation = 5.0 V peak to peak.

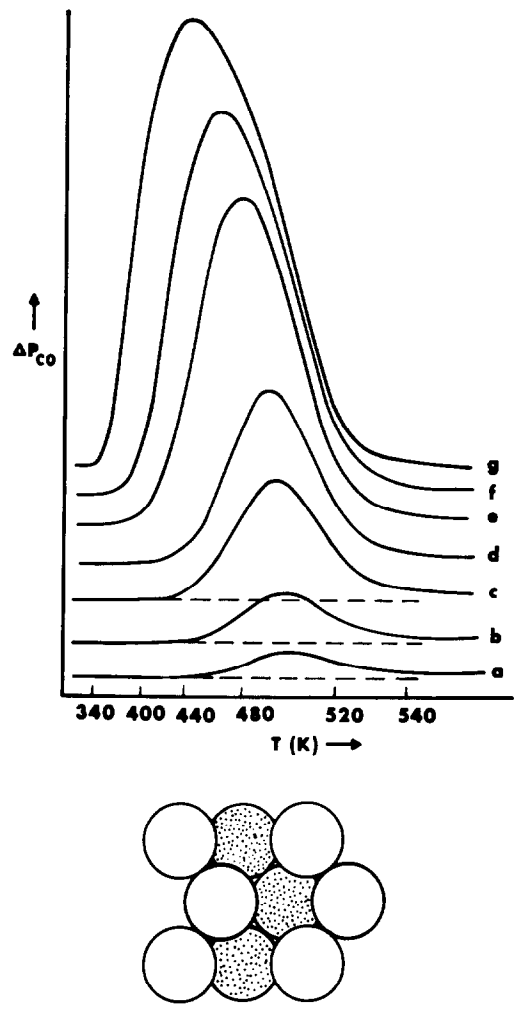

FIG. 3. Flash-desorption spectra following adsorption of CO on Ru(110) at ~300 K. The CO exposures corresponding to each spectrum were: (a) 0.13, (b) 0.25, (c) 0.47, (d) 0.68, (e) 1.3, (f) 1.9, (g) 6.8 Langmuirs. A mode of the kinked Ru(110) surface is shown below.

26.9 to ~22.8 kcal/mol over the range of CO coverages shown in Fig. 3. The temperature range of CO desorption on Ru(110) (~350–550 K) is virtually identical to that observed for CO desorption from the close-packed Ru(001) plane (*8*) and from the more rough Ru(101) plane (*10*). Two well-resolved CO binding states are observed on Ru(001), and two less clearly resolved states are seen on Ru(101).

Flash-desorption spectra for H_2 on Ru(110) are shown in Fig. 4. It should be noted that, at 300 K, a saturation coverage of H_2 is much smaller than CO. The major portion of H_2 desorbs below 300 K; thus, these spectra represent the adsorbed H_2 species having the highest adsorption energy. The dotted line corresponds to a theoretical fit to the data based upon first-order desorption kinetics, where the slight convexity of the leading edge of the experimental curves has been ignored. The desorption energy, E_d, found using a pre-exponential factor of 1×10^{-12} sec^{-1}, is 17.5 kcal/mol. The monotonic buildup above $\theta = 0.5$ is consistent with first-order desorption kinetics. Desorption data were collected following adsorption of a 1:1 H_2/D_2 mixture. The results confirmed complete statistical scrambling, thus implying that this desorption state is due to adsorbed H atoms. Recent studies of H_2 desorption from Ru(110) following adsorption at 80 K indicate that desorption proceeds via second order kinetics at higher hydrogen coverages (*11*).

Figure 5 shows the results of the addition of CO to a saturated H_2 layer. There is

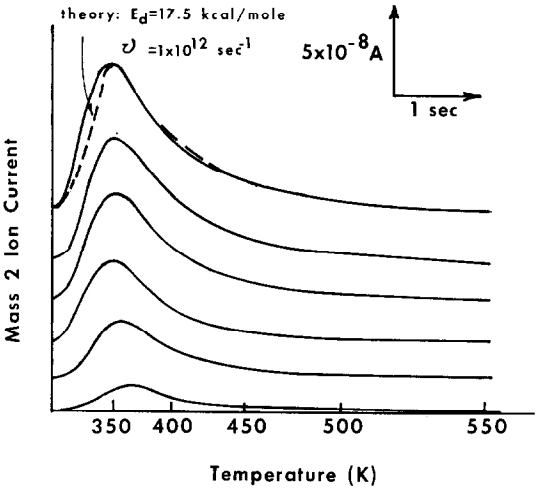

FIG. 4. H_2 desorption from Ru(110). Flash-desorption spectra for increasing coverage of H_2 on Ru(110) up to a saturation coverage.

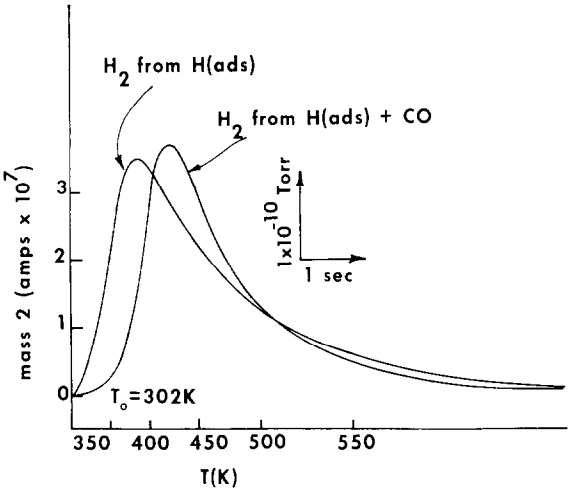

FIG. 5. Interactions of saturated hydrogen monolayer with CO on Ru(110). Carbon monoxide-induced displacement of H_2 thermal desorption spectrum. (Left) H_2 from saturation coverage of H_2. (Right) H_2 at saturation coverage after being subjected to a saturation exposure of CO.

clearly a positive interaction causing the H_2 desorption peak to shift to higher temperatures, implying that, for a constant pre-exponential factor, the binding energy increases by 2–3 kcal/mol. Alternatively, this shift could be explained by a factor of ten change in the preexponential factor of the desorption of the two states. This agrees with the work of McKee (*12*) on ruthenium films where, similarly, a positive CO–H interaction was observed. This positive interaction interestingly contrasts with the adsorption of CO, in which a CO–CO repulsive interaction is seen (*8*). Kraemer and Menzel (*13*) have also reported evidence for CO–hydrogen interactions in measurements of work function changes on Ru field emitters at 300 K.

This positive CO–H interaction suggested that perhaps methane could be formed upon thermal desorption of coadsorbed H_2 and CO. A very careful examination of the thermal desorption products from mixed H–CO layers at the highest possible sensitivity indicated the absence of any detectable methane production at a sensitivity level of $\sim 10^{-4}$ monolayers. Going further, a search was carried out at higher H_2/CO incident flux. The crystal was exposed to a H_2/CO mixture (4:1) at a steady-state flux equivalent to a pressure of 10^{-3} Torr via the molecular beam. Then, monitoring again with the highest sensitivity for methane, the crystal temperature was varied. The results of this experiment are displayed in Fig. 6. The limits of sensitivity in this experiment were such that a local pressure of 4×10^{-10} Torr of CH_4, generated in the region of the crystal, could be detected using the QMS. Based on the equilibrium constant for the methanation reaction, the equilibrium partial pressure of methane in a 4:1 H_2/CO mixture at a total pressure of 10^{-3} Torr and temperature of 600 K is calculated to be 6×10^{-7} Torr. Thus, the upper limit on the rate of CH_4 production at 600 K, shown in Fig. 6, is $\sim$1000 times less than the thermodynamic limit. This is clearly due to kinetic limitations in the rate of formation of CH_4 from H_2 + CO over Ru. Ancillary experiments up to 1400 K were also negative for CH_4 production.

After demonstrating that the rate of methane production from H_2 and CO was too low to be measured under pressure

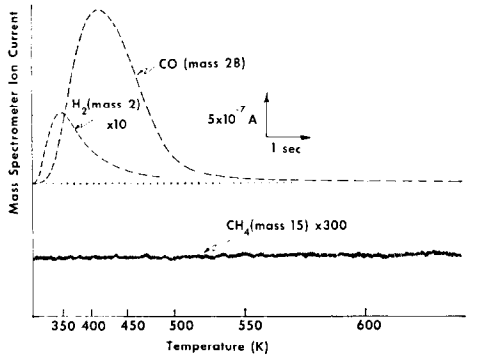

FIG. 6. Study of CH_4 production (below) from Ru(110) in an $H_2 + CO$ beam, demonstrating the lack of evidence for CH_4 production. The beam flux corresponded to a local $H_2 + CO$ pressure of $\sim 10^{-3}$ Torr. For reference, the flash-desorption spectra of CO and H_2 after a saturation exposure of the pure gas are shown above at the noted sensitivities.

conditions attainable here, we attempted to study the chemistry of formaldehyde on the same crystal plane. Of particular interest are the CO hydrogenation products because of the possible population enhancement of such product precursors which might be formaldehyde-like in nature.

Figure 7 illustrates what happens kinetically when a formaldehyde beam strikes a Ru(110) crystal. As the clean crystal is rotated into the formaldehyde molecular beam, gas evolution or adsorption is monitored with the QMS. The lower trace (mass 29) is indicative of formaldehyde uptake. As the clean crystal is rotated into the beam, the background partial pressure of formaldehyde decreases, because the crystal intercepts $\sim 20\%$ of the H_2CO molecules from the doser. As the coverage on the crystal increases, the rate of adsorption drops off until after 50–60 sec, when the crystal becomes saturated. The upper trace shows that, simultaneously with formaldehyde uptake, H_2 gas (mass 2) is evolved from the crystal. A similar experiment monitoring mass 28 indicated no CO evolution. Thus, at 300°K, at least some of the formaldehyde dissociates upon interaction with the crystal with concurrent evolution of H_2. The concomitantly formed CO remains on the surface.

Some H_2, however, is retained on the crystal following formaldehyde chemisorption. Figure 8 shows a comparison of the H_2 observed in thermal desorption of a formaldehyde layer and the H_2 from a pure hydrogen layer. In the formaldehyde case, the peak in the hydrogen desorption spectrum shifts to higher temperature, indicating a higher E_d, reminiscent of the positive H–CO interaction previously shown in Fig. 5. In addition, there is significantly more H_2 on the surface from

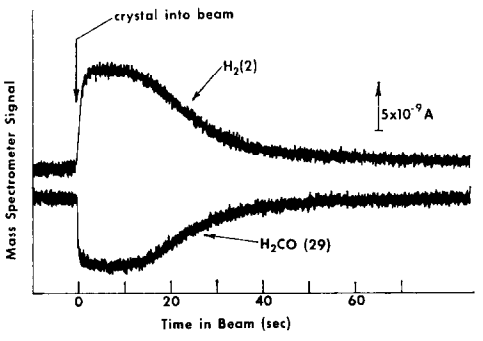

FIG. 7. Dynamics of H_2CO adsorption on Ru(110) using a molecular beam. Each curve is a direct tracing of an x–y recorder plot of QMS signal versus time as the clean Ru(110) crystal intercepts an H_2CO beam.

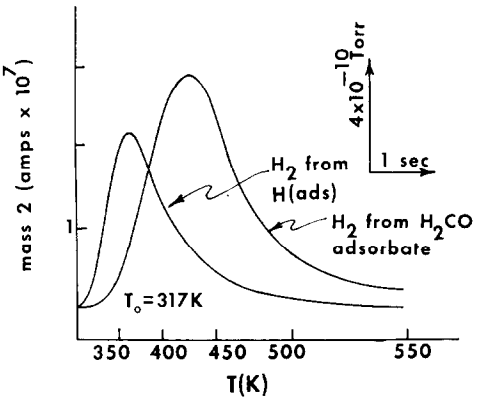

FIG. 8. A comparison of the flash-desorption spectra of H_2 after a saturation exposure to H_2 (left) and H_2CO (right) at ~ 300 K.

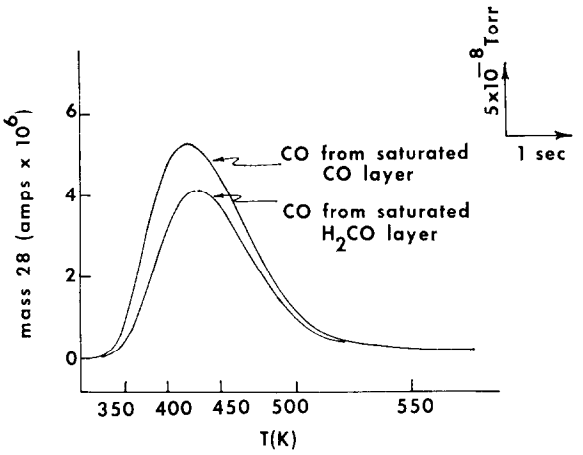

FIG. 9. Flash-desorption spectra comparing CO desorption from a CO monolayer and from a saturated H_2CO layer on Ru(110).

the formaldehyde adsorbate as compared with pure H_2. It appears that, upon interaction with the Ru(110) surface, almost all of the formaldehyde dissociates into adsorbed H_2 and adsorbed CO. In turn, most of the H_2 is liberated as H_2(g). The remaining H has its binding energy increased through interaction with the adsorbed CO as in the case of coadsorbed H_2 and CO. This increase in binding energy may be responsible for the observed increase in saturation hydrogen coverage as compared with pure hydrogen. In addition, the possibility of a low-coverage complex containing H and CO cannot be excluded as the source of some additional hydrogen in this experiment. An observation supporting this latter viewpoint is the fact that the hydrogen coverage could *not* be increased by coadsorption of H_2 and CO, where a binding energy increase for adsorbed hydrogen was also observed.

The CO retained on the Ru(110) surface after a formaldehyde saturation exposure is observed to be *less* than that found for pure CO. This difference is displayed in Fig. 9. Apparently, certain sites which are easily populated by pure CO remain unoccupied or are occupied very slowly with the decomposition of formaldehyde. This is confirmed by the observation that CO sites remaining unoccupied after formaldehyde decomposition could be filled by adsorption of pure CO. This phenomenon could easily arise because of the steric problems that would necessarily be associated with formaldehyde decomposition at sites not readily accessible, i.e., the bottom of kinks.

In marked contrast to coadsorbed H_2 and CO, the formaldehyde adsorbate, upon desorption, gives rise to small amounts of additional products other than H_2 and CO. These results indicate that at least small amounts of other species are present on the crystal when formaldehyde is the adsorbate which are not present when H_2 and CO mixtures are adsorbed. Figure 10 displays the relative abundance of desorption products. Assigning a yield of 100% to CO, the H_2 yield is seen to be near 10%, whereas the remaining products fall into the 1–0.1% yield range. Although, relative to CO, the yields of H_2CO, CO_2, H_2O, and CH_4 are small, the amounts of CH_4, CO_2, and H_2O are sizable compared to the yield of formaldehyde.

It should be emphasized that these minor products are certainly significant in view of the fact that no detectable amounts of any of these compounds are observed with mixtures of H_2 and CO.

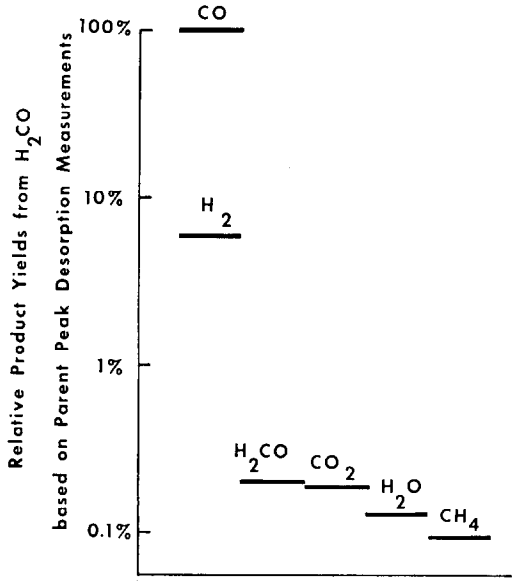

FIG. 10. Relative yields of the desorbing product from Ru(110) after a saturation exposure to H_2CO at ~300 K.

It should also be noted that the yields in Fig. 10 are raw experimental yields determined by a time integration of the QMS ion current for the particular mass peak of interest (CH_4: mass 15; H_2CO: mass 30). The yields are uncorrected for pumping speed, QMS sensitivity, etc.

Figure 11 displays the normalized yields of the desorption products as a function of the formaldehyde dosing time. (The dosing rate is lower than for the uptake experiment of Fig. 7.) Each plot represents the fractional yield as compared with the saturation yield. The H_2 and CO rise smoothly together until the crystal saturates at about 600-sec of beam dosing time. Interestingly, the CH_4 production is not detectable until about 30% of the surface is covered with H and CO decomposition products from formaldehyde. Thus, CH_4 production probably involves a species originating from formaldehyde, which is only stable on the surface at later stages of H(ads) and CO(ads) coverage.

In Fig. 12 are found the normalized desorption yields of H_2CO, CO_2, and H_2O. The buildup of these products is seen to be intermediate in rate to the CO and CH_4 yield curves.

The desorption curves of CH_4, CO_2, H_2O, and H_2CO are shown in Fig. 13 to illustrate their size and thermal desorption profiles.

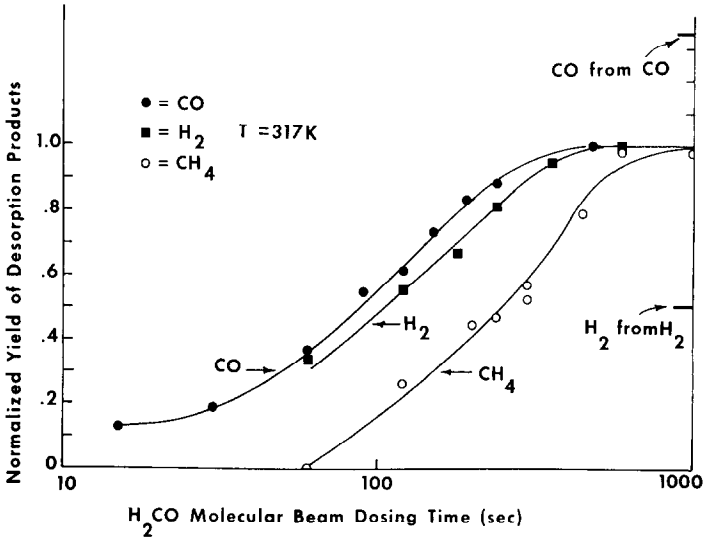

FIG. 11. Normalized desorption yields of CO, H_2, and CH_4 on Ru(110) as a function of exposure time to a H_2CO molecular beam.

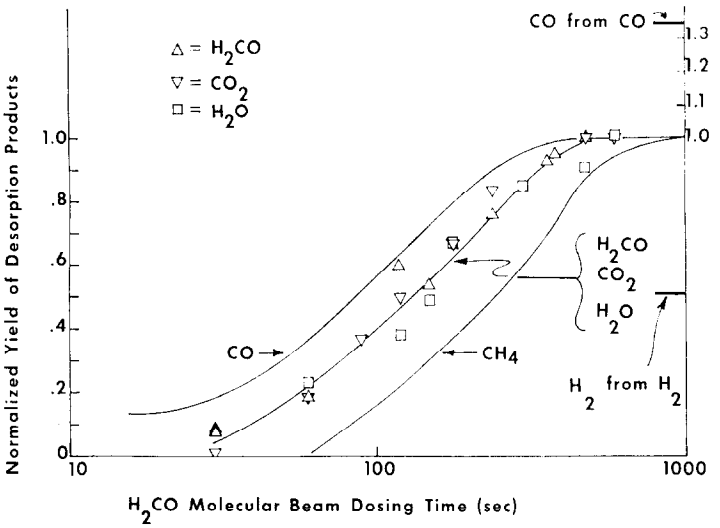

FIG. 12. Normalized yields of H_2CO, CO_2, and H_2O on Ru(110) as a function of exposure to a H_2CO molecular beam.

The maximum of each falls into a narrow temperature regime, suggesting the possibility that there is an interrelation between the processes yielding all of these species.

DISCUSSION

The first point to address concerns the reason for the reduction in CO desorption energy, E_d, from Ru(110) as a function of increasing coverage, θ_{CO}. It is instructive to consider the previous CO adsorption studies on other Ru surfaces. On both Ru(001) and (101) surfaces, two CO binding states are seen in thermal desorption studies; the state having lower binding energy populates at higher coverages. On Ru(001), the correlation of LEED (*8*), thermal desorption (*8*), UPS, and XPS (*14*), studies indicates that, at low CO coverages, only one binding state is present which is characterized by an ordered LEED structure at 300 K. At higher coverages, repulsive CO–CO interactions cause the layer to disorder and result in the appearance of a second binding state having reduced binding energy in the thermal desorption spectra. On Ru(101), the situation is somewhat different (*10*). Adsorption at low coverages results in no new LEED structure forming at 300 K; at higher exposures, the CO layer forms an ordered structure which persists to saturation coverage. The two binding states seen in thermal desorption are reasoned to originate from adsorption of CO on different sites, *not* simply from repulsive interactions. This suggestion is supported (*10*) by

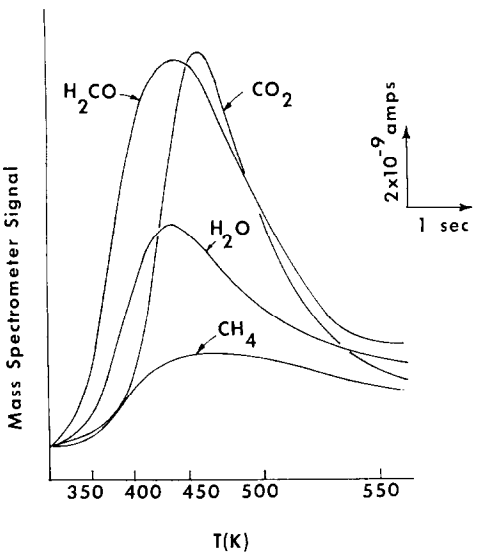

FIG. 13. Flash-desorption spectra of CH_4, H_2CO, CO_2, and H_2O on Ru(110) after a saturation exposure to H_2CO.

electron-stimulated desorption studies, and by studies of CO coadsorbed with carbon or oxygen on Ru(101). The results are not unambiguous, however, and the "order–disorder" vs "separate site" origin for the binding states on Ru(101) can probably best be resolved using a spectroscopic method such as UPS or vibrational spectroscopy.

LEED studies (*15*) of CO on the Ru(110) surface at 300 K show greater similarity to Ru(101) than to Ru(001). At low CO coverages, no new LEED features are seen; at high CO coverages, an ordered CO overlayer forms which persists to saturation coverage. UPS studies (*16*) of CO on Ru(110) indicate that there is no detectable change in the molecular orbital structure between low and high CO coverages; the familiar 4σ and $(5\sigma + 1\pi)$ levels are observed at all coverages. If CO on Ru(110) is adsorbed on two types of sites at high θ_{CO}, this difference cannot be resolved using UPS, although a more sensitive form of spectroscopy (e.g., vibrational spectroscopy) might detect such a difference. For the present, we cannot exclude the possibility of adsorption on different sites at high θ_{CO} on Ru(110), but the general observation of "crowding" and repulsive interactions in mobile CO layers at high coverages on other metal surfaces (*17*) suggests that repulsive CO–CO interactions may be a more likely explanation of the decrease in E_d with θ_{CO} on Ru(110).

In contrast to the CO–CO repulsive interaction, coadsorbed H_2 and CO on Ru(110) exhibit a positive interaction, resulting in an increase in the H_2 desorption energy. This interaction, however, is insufficient to produce any observable hydrocarbon product and, therefore, is not attributable to a surface complex formed between H(ads) and CO(ads). In fact, in $H_2 + CO$ mixtures at steady-state pressures of 10^{-3} Torr, CH_4 production was observed to be less than 1 part CH_4 for 10^6 parts $(CO + H_2)$.

Conrad *et al.* (*18*) have studied H_2–CO interactions on a single-crystal(111) surface of Ni (another metal known to be an excellent methanation catalyst). They noted that, at low H coverages, interaction with adsorbed CO caused a conversion to a more *weakly* bound hydrogen state, designated β'. In contrast, at high H coverages, where repulsive H–H interactions produce a lower binding energy form of hydrogen state, interaction with adsorbed CO causes a conversion to the more *strongly* bound β'-hydrogen state. In both cases, energetic changes of about ± 2 kcal/mol are caused by the CO–H interaction. These effects are thought to be related to slight conformational changes induced by coadsorption of the dissimilar species, with little or no effect on the CO valence orbitals, i.e., evidence for a chemical complex is absent. Similar CO–H *attractive* interactions have been observed calorimetrically by Wedler (*19*) in coadsorption studies on evaporated Ni films at all hydrogen coverages for $\theta_{CO} = 0.1$. In summary, the *positive* CO–H interaction observed on Ru(110) at low hydrogen coverages seems to be absent for low-hydrogen coverage layers on Ni(111), but is seen at high hydrogen coverages on Ni(111) and at both high and low hydrogen coverages on polycrystalline Ni films.

Another difference between Ni and Ru surfaces concerns their interaction with CO. It is known that heating a Ni crystal to $\lesssim 400$ K in CO at pressures as low as 10^{-7} Torr results in a buildup of surface carbon, accompanied by the evolution of CO_2 via the disproportionation reaction

$$2\,CO \rightleftharpoons C(s) + CO_2(g).$$

Wentrcek *et al.* (*20*) and Araki and Ponec (*21*) have demonstrated that the carbon deposited on Ni surfaces via the disproportionation reaction can be subsequently hydrogenated to form methane. They further concluded that the rate-limiting step in the catalytic hydrogenation of CO

by Ni to form methane is the dissociation of CO to form this "active" form of surface carbon. This carbon is not in the same form as in bulk nickel carbide (Ni_3C), which is known to be a poor methanation catalyst.

On the other hand, heating a Ru(110) crystal to 630 K at a CO pressure of 2×10^{-3} Torr for 30 min (total CO exposure of 3.6×10^6 Langmuir) did *not* result in the appearance of surface carbon as detected using Auger electron spectroscopy. Previous results (*8*) for CO on Ru(001) also indicated no detectable CO dissociation at temperatures and pressures as high as 700 K and 10^{-4} Torr, respectively. Adsorbed CO on Ru is easily dissociated by low-energy electron bombardment (*8*, *10*), however, and this phenomenon has been studied in considerable detail recently (*22*). (It would be of interest to see if the carbon produced in this fashion can be hydrogenated to form CH_4.) Although we cannot eliminate the possibility of CO dissociation on Ru catalysts at the higher pressures used in practical methanation catalysis, it is clear that there are substantial quantitative differences in the rate of CO dissociation and subsequent carbon accumulation on the surfaces of the two metals. This difference is further evidence that the mechanism of the catalytic methanation reaction may be different on the two metals. We discuss below the evidence for a possible oxygenated hydrocarbon intermediate for methanation on Ru.

Formaldehyde incident on a clean Ru(110) crystal yields primarily H_2(g) and CO(ads). In addition, H(ads) plus oxygenated species are also present. Desorption yields principally H_2 and CO, with traces of CH_4, CO_2, H_2O, and H_2CO. Presumably, these latter products arise from the thermal decomposition of the oxygenated hydrocarbon species. These minor products might constitute only a small fraction of the decomposition products of this hydrocarbon precursor, the remainder yielding H_2 and CO. Thus, the population of this intermediate could be substantially larger than might be inferred from the relative abundance of methane product. Preliminary UPS (*23*) and ESCA data, however, indicate no detectable oxygenated carbon species other than CO for this system at 300°K. Therefore, the population of surface complexes derived from H_2CO is assumed to be less than a few percent of a monolayer.

Finally, of particular interest is the fact that CH_4 is not observed to form until the latter stages of formaldehyde adsorption. This implies a prerequisite hydrogen-rich environment for CH_4 production or, as suggested in previous publications (*4*, *5*), formation of a surface complex arising from a bimolecular surface reaction.

The striking feature of the formaldehyde system, as opposed to a mixture of H_2 and CO, is that methane, water, and carbon dioxide are observed. Therefore, it is quite likely that formaldehyde or some species derived from formaldehyde may well be involved as an intermediate in methanation over ruthenium. Final judgement as to the specific nature of this surface intermediate must await further studies.

SUMMARY OF RESULTS FOR ADSORPTION ON Ru(110)

(i) As CO coverage increases on Ru(110), the CO binding energy decreases. (ii) Coadsorption of hydrogen and CO results in an increase in the hydrogen desorption energy in comparison to desorption from a pure hydrogen layer. (iii) No detectable methane is produced when the Ru(110) crystal is heated in a 4:1 H_2/CO mixture at 10^{-3} Torr in the temperature range of 300–1400 K. (iv) The adsorption of H_2CO on Ru(110) is mainly dissociative, with the major desorption products being H_2 and CO. (v) Following a large dose of H_2CO, additional thermal desorption products include H_2O, H_2CO, CO_2, and CH_4 at the 0.1% level.

ACKNOWLEDGMENT

The authors acknowledge with pleasure the support of this work by the Energy Research and Development Administration through the Office of Molecular, Mathematical and Geosciences, Division of Physical Research.

REFERENCES

1. Mills, G. A., and Steffgen, F. W., *Catal. Rev.*, **8**(2), 159 (1973).
2. Vannice, M. A., *J. Catal.* **44**, 152 (1976).
3. Dalla Betta, R. A., Piken, A. G., and Shelef, M., *J. Catal.* **35**, 54 (1974); **40**, 173 (1975).
4. Yates, J. T., Jr., Madey, T. E., and Dresser, M. J., *J. Catal.* **30**, 260 (1973).
5. Worley, S. D., Erickson, N. E., Madey, T. E., and Yates, J. T., Jr., *J. Electron Spectrosc.* **9**, 355 (1976).
6. Worley, S. D., and Yates, J. T., Jr., *J. Catal.*, to be published.
7. Palmberg, P. W., Riach, G. E., Weber, R. E., and MacDonald, N. C., "Handbook of Auger Electron Spectroscopy." Physical Electronics Industries, Edina, Minn., 55435, 1972.
8. Madey, T. E., and Menzel, D., *Japan. J. Appl. Phys.*, Suppl. 2, Part 2, 229 (1974).
9. Madey, T. E., and Yates, J. T., Jr., *Surface Sci.* **63**, 203 (1977).
10. Reed, P. H., Comrie, C. M., and Lambert, R. M., *Surface Sci.* **59**, 33 (1976).
11. Goodman, D. W., Yates, J. T., Jr., Madey, T. E., and Fisher, G. B., unpublished data.
12. McKee, D. W., *J. Catal.* **8**, 240 (1967).
13. Kraemer, K., and Menzel, D., *Ber. Bunsenges. Phys. Chem.* **79**, 649 (1975).
14. Fuggle, J. C., Madey, T. E., Steinkilberg, M., and Menzel, D., *Surface Sci.* **52**, 521 (1975).
15. Carroll, J. J., Melmed, A. J., Madey, T. E., Sandstrom, D. R., and Ono, M., unpublished data.
16. Sandstrom, D. R., Vorburger, T. V., and Waclawski, B. J., to be published.
17. Tracy, J. C., *J. Chem. Phys.* **56**, 2736 (1972); **56**, 2748 (1972).
18. Conrad, H., Ertl, G., Kuppers, J., and Latta, E., *in* "Proceedings, International Catalysis Congress, London, 1976, p. 1.
19. Wedler, G., Papp, H., and Schroll, G., *J. Catal.* **38**, 153 (1975).
20. Wentrcek, P. R., Wood, B. J., and Wise, H., *J. Catal.* **43**, 363 (1976).
21. Araki, M., and Ponec, V., *J. Catal.* **44**, 439 (1976).
22. Umbach, H., Fuggle, J. C., Feulner, P., and Menzel, D., *Surface Sci.* **64**, 69 (1977).
23. Fisher, G. B., Yates, J. T., Jr., Madey, T. E., to be published.